
Scalable Computing: Practice and Experience, ISSN 1895-1767, http://www.scpe.org
 Volume 25, Issues 6, pp. 5184–5196, DOI 10.12694/scpe.v25i6.3263

MATHEMATICAL NONLINEAR GRAPH THEORY TOPOLOGY LAYER MODEL FOR PHOTOELECTRIC TRACKING SYSTEM

JING LI* AND YUNPENG SHANG†

Abstract. The performance of the photoelectric tracking system mainly depends on the tracking accuracy. In order to achieve the purpose of high precision tracking, controlling the power dragging device, the main component of the photoelectric tracking system, is the main means to achieve this purpose. In order to improve the tracking speed and accuracy of photoelectric tracking systems, the author proposed a mathematical nonlinear graph theory topology layer model for photoelectric tracking systems. The topology layer model and the motion node servo mechanism model of the photoelectric tracking system are studied, and the two-stage disturbance sources that affect the tracking stability are analyzed. The results show that the interference estimation error range designed by the author reaches 3×10^{-3} through comparison, it can be seen that the estimation error designed by the author is significantly smaller than the ESO estimation error, and the buffeting is small. Through comparison, it can be concluded that the estimation error of the algorithm and the disturbance observer designed by the author are significantly smaller than the estimation error of ESO, and the buffeting is small, and they have strong compensation ability for the disturbance of different frequencies. The interference observer can quickly and accurately estimate the interference and prove its stability. The effectiveness of the proposed observer and disturbance observer is fully demonstrated. The finite time integrated site selection mode disturbance observer (F-ISMDOB) is designed to quickly estimate and compensate for equivalent interference, and effectively improves the anti-interference performance of the system structure layer.

Key words: Photoelectric tracking system, Collaborative control, Tracking differentiator, Finite-time convergence, Sliding mode control, Graph theory topological layer model

1. Introduction. Photoelectric tracking system is a high-precision acquisition and tracking equipment with multi-disciplinary integration, such as optics, mechanical design, power electronics, signal processing, etc, it is commonly used in range measurement, spacecraft orbit determination, laser communication and target tracking and other applications. Photoelectric tracking servo control system mainly includes: photoelectric detection, signal processing, intelligent control and mechanical device and other parts. Its main function is to control the motor drive tracking axis according to the target position deviation signal, to achieve real-time, high-precision tracking of the target, which has been widely used in both military and civilian fields. In order to achieve high-precision tracking of the target, the traditional photoelectric tracking system generally adopts the composite axis control technology, including two tracking units of rack and precision tracking platform[1]. The rack system drives the actuator of the rack according to the tracking error of the coarse detector with large field of view and low resolution to complete the primary coarse tracking; Because the classical control method cannot accurately calculate the actual operation trajectory of the target, some new intelligent control methods and the hybrid control formed by mutual fusion are applied, which improves the stability of the target tracking. Examples are multi-mirror systems and systems. The high-resolution precision detector detects the residual error of the first-level tracking, and uses the precision tracking platform to complete the real-time tracking of the target to obtain the final tracking accuracy of the photoelectric tracking system. With the continuous expansion of the application field of photoelectric tracking system, photoelectric tracking systems with different mechanical structures are gradually emerging[2].

Composite axis tracking control is an effective means to improve the tracking accuracy of the photoelectric tracking system at present, and its core is the collaborative work of two levels of coarse and fine tracking. Photoelectric capture and tracking devices are often equipped with astronomical telescopes, weapon control

*School of Computer Engineering, Guangzhou City University of Technology, Guangzhou, Guangdong, 510800, China (Corresponding author, JingLi62@126.com)

†School of Computer Engineering, Guangzhou City University of Technology, Guangzhou, Guangdong, 510800, China (YunpengShang6@163.com)

systems and other photoelectric measurement equipment, in order to quickly achieve the purpose of discovery and accurate tracking targets. The servo tracking system is mainly to quickly capture and continuously track the identified target, or to guide the target into the capture field of view. On the basis of the precise positioning of the rack servo system, the primary coarse tracking ensures that the tracking residual is within the compensation range of the secondary fine tracking according to the close-loop of the coarse TV miss distance, so as to achieve the final desired tracking accuracy. Generally, the control loop of the rack positioning link in the primary coarse tracking consists of three closed loops, namely, current-inertia-positioning[3]. The current control circuit determines the action torque when the frame rotates, and its performance is determined by many aspects, such as motor selection, control algorithm design and hardware matching; The inertial loop uses inertial sensors, such as speed measuring gyroscope and accelerometer, in order to make the actuator stable relative to the inertial space, so as to achieve the effect of resisting disturbance; The photoelectric tracking servo system processes the instructions, state and error signals from the image processing computer, main control computer, gyroscope, rotating transformer and other components, and processed through the digital signal processor to rotate the motor of the drive turntable to realize the stable and accurate tracking of the photoelectric tracker. Generally, a multi-closed-loop cascade composite control structure, including current loop, rate loop and position loop, is used to meet the needs of the system for fast response, high-precision tracking and reliability control. The positioning loop designs the controller according to the positioning residual to ensure that the positioning residual is small enough to complete the secondary precision tracking. Similarly, the precision tracking platform matched with the secondary precision tracking is also composed of a current-velocity-tracking three-loop control circuit, the motors of the precision tracking platform are generally piezoelectric ceramics, voice coil motor and giant magnetostrictive actuator; Inertia loop is used for anti-interference; The key of secondary precision tracking is the control algorithm design of the tracking loop, which determines the final pointing accuracy of the photoelectric tracking system[4]. Conventional control technology is widely used in practical industrial activities because of its simple principle and good stability. However, the conventional time-varying and non-linear system cannot achieve the purpose of precise control, so it is difficult to maximize its role. It is a new stage to solve the control problem of complex system, realize rapid response and smooth transition and other advantages of the development of intelligent control.

2. Literature review. Because of its unique strategic significance in military field, photoelectric tracking system has always been a hot research topic at home and abroad. In 1915, the aerial camera was first used in aerial reconnaissance, opening the application of airborne camera. The research status of optoelectronic tracking platform system and optoelectronic tracking and stabilization platform system LOS stability control are introduced respectively. The original photoelectric tracking platform was designed to be used as the eyes of aircraft for military reconnaissance. Later, due to the lack of real-time aerial cameras, which can not meet the needs of the battlefield, the development of new photoelectric platforms has become a research hotspot in various countries. The fuzzy controller is used to reason about the controlled object, and the dynamic characteristics and performance indexes of the controlled object are described by fuzzy language and rules, so as to realize the method of controlling the system is called fuzzy control. Fuzzy control system is a control process that simulates human reasoning and decision-making based on fuzzy control theory and taking empirical knowledge and expert control as the control rules. Fuzzy control uses fuzzy logic reasoning, fuzzy set theory and fuzzy language variables, and it is an intelligent control system that replaces human operation through computer control technology. At the same time, optics, electronics, automatic control technology and computer technology have also developed vigorously. In recent years, countries around the world have taken the research of optoelectronic stabilization platform as an important research content, and constantly seek new control technologies to improve scientific research capabilities, the United States, Israel and other countries have made many research achievements and developed relatively rapidly[5]. At the beginning of the 1970s, the photoelectric imaging equipment developed by Israel sent the images on the UAV back to the ground for the first time, opening the precedent of the research on the photoelectric stabilization platform. The stabilized platform can keep the optical equipment on it relatively stable, and is widely used in the optoelectronic pod system. The photoelectric pod is the most important part of the photoelectric tracking system, the photoelectric pod carried on the UAV can replace people to carry out reconnaissance tasks, improving human security. The photoelectric pod can be widely used in land, sea, air and space reconnaissance, and its carrier is vehicles, ships,

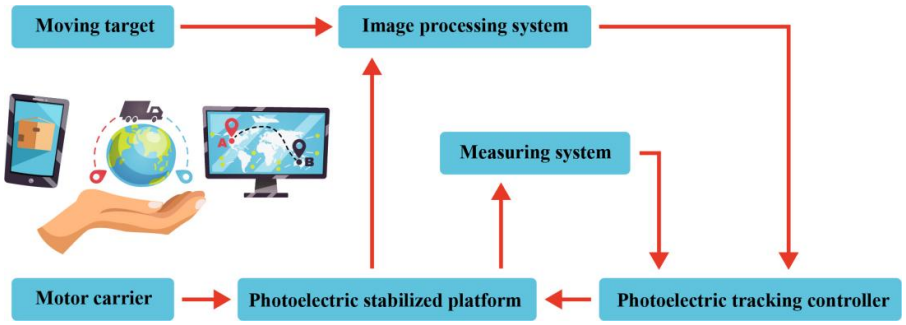

Fig. 3.1: Schematic diagram of photoelectric tracking imaging system

aircraft and satellites. Tong, W proposed two non-single interval type 2 fuzzy PID (NIT2F-PID) controllers for high-precision photoelectric tracking system (ETS) to improve its anti-interference ability [6]. Bao, G studied the latest progress of cooperative control of constrained heterogeneous multi-agent systems [7]. Ziquan, Y. introduced the latest development of fault-tolerant cooperative control (FTCC) for multiple unmanned aerial vehicles (UAVs)[8].

To improve the tracking speed and accuracy of the photoelectric tracking system. The author aims at the problem that the distributed cooperative control system does not measure the speed and has interference. First, combined with the advantages of the super-spiral anti-buffeting, a finite-time super-twisting observer (F-SO) is proposed to estimate the state information of the system structure layer quickly and accurately; Secondly, the Finite-time Integral Siting Mode Disturbance Observer (F-ISMDOB) is designed to quickly estimate and compensate the equivalent interference, thus effectively improving the anti-interference performance of the system structure layer. The results show that the interference estimation error range designed by the author reaches 3×10-3 through comparison, it can be seen that the estimation error designed by the author is significantly smaller than the ESO estimation error, and the buffeting is small.

3. Research methods.

3.1. Structure of photoelectric tracking system. The platform structure of the photoelectric tracking system is composed of the pitch axis, the azimuth axis, the gyroscope, the drive motor and the relevant optical equipment. The basic principle of the photoelectric tracking system is: to calculate and process the position deviation signal of the target and send it to the loop control unit to control the motor drive turntable, so that the photoelectric sensor can realize automatic tracking. The system can also turn the turntable according to the predetermined requirements. Due to the mobility performance of the target and the stability and tracking requirements of photoelectric tracking, the power drag control technology of servo turntable has become the key technology of the system. The so-called electric drag control, namely for the speed control of the motor and mechanical equipment, so that the rotation speed can be freely adjusted. In order to ensure the normal operation of the system, it is necessary to understand the mechanical characteristics and process characteristics of the motor and load equipment. Based on the brief introduction of the system stability control method, as shown in Figure 3.1, the photoelectric tracking imaging system. When the system is working, the miss distance information is calculated by the computer, the data is detected in real time by the sensor, and the input and output deviation error is obtained, and then the unified cooperative control algorithm is used to track it in real time, while weakening and isolating all kinds of interference received by the system, so as to make the optical equipment stable imaging [9].

From the above analysis of optoelectronic equipment structure and imaging mechanism, the optoelectronic tracking system is composed of several typical servo mechanisms. Field of view of moving target CCD camera, through the image processing system, the target miss distance information is sent to the servo control mechanism of the pitch and azimuth axes, which drives the frame to move, and then makes the LOS close to the target point; At the same time, the image processing system transmits the detected miss distance difference information

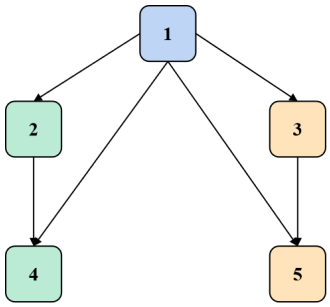

Fig. 3.2: Topological structure

to the servo actuator of the fast mirror, which includes the pitch and azimuth two axis structure, the fast mirror realizes the purpose of fast tracking and understanding the target through the compensation of tracking deviation; The measuring equipment further corrects the system control error by measuring the output value as the system feedback [10].

3.2. Modeling of photoelectric tracking system network structure.

3.2.1. System network structure modeling. The photoelectric tracking system is mainly used to complete the target search and automatic or automatic (semi-automatic) tracking functions, and accurately points to the target for the carrying task equipment. Through the feedback of Angle measuring elements and infrared tracker, and the rotation Angle of the azimuth axis and pitch axis is controlled, so as to complete the real-time tracking of the moving target. From the perspective of the overall structure of the photoelectric tracking system, according to the actual situation of the connection and communication mode of each actuator of the system and the tracking, the overall structure model and kinematics model of the photoelectric tracking system are established by using topological structure, algebraic graph theory and matrix; Taking the expected acceleration as the bridge connecting the whole structure and the actuators, the kinematic model of the actuator with moving nodes is established [11].

In the topological network structure model of the system, the nodes in the figure represent the moving target and each actuator of the photoelectric tracking system (the azimuth and pitch axes of the execution frame, the azimuth and pitch axes of the fast mirror), the edge in the figure represents the information transmission and connection mode between various actuators, and the direction of the edge represents the logic or information transmission direction.

As shown in Figure 3.2, the topological structure of the photoelectric tracking system with two axes and two frames, node 1 represents the moving target, and nodes 2 and 3 represent the pitch axis and azimuth axis of the photoelectric tracking system respectively, the target is directly tracked, nodes 4 and 5 represent the pitch axis and azimuth axis of the fast mirror, respectively, and track the residual error of the tracking moving target quickly [12].

According to the matrix theory, the topological structure of the system is transformed into a matrix, and the network structure of the photoelectric tracking system is expressed in the form of matrix, such as adjacency matrix, penetration matrix, Laplace matrix, etc.

$$\text{Adjacency matrix: } A = \begin{bmatrix} 0 & 0 & 0 & 0 & 0 \\ 1 & 0 & 0 & 0 & 0 \\ 1 & 0 & 0 & 0 & 0 \\ 1 & 1 & 0 & 0 & 0 \\ 1 & 1 & 0 & 0 & 0 \end{bmatrix}$$

Penetration matrix (diagonal matrix): $D = \begin{bmatrix} 0 & 0 & 0 & 0 & 0 \\ 0 & 1 & 0 & 0 & 0 \\ 0 & 0 & 1 & 0 & 0 \\ 0 & 0 & 0 & 2 & 0 \\ 0 & 0 & 0 & 0 & 2 \end{bmatrix}$

Laplacian matrix: $L = D - A = \begin{bmatrix} 0 & 0 & 0 & 0 & 0 \\ -1 & 1 & 0 & 0 & 0 \\ -1 & 0 & 1 & 0 & 0 \\ -1 & -1 & 0 & 2 & 0 \\ -1 & -1 & 0 & 0 & 2 \end{bmatrix}$

The first-order kinematics model of each node including the moving target point is described as follows 3.1:

$$\dot{x}_i = u_i, i = 1, 2, \cdots, n \tag{3.1}$$

where $x_i \in R$ represents the position status of actuator i, and $u_i \in R$ represents the control input of actuator i.

Since the photoelectric tracking system and its tracking target point are second-order kinematics models, the structural kinematics model can be described as follows 3.2:

$$\dot{x}_i = u_i, i = 1, 2, \cdots, n \tag{3.2}$$

where x_i and v_i represent the position status and speed status of the actuator i, u_i represents the control input of the actuator, and d_i represents the interference of the actuator i.

The photoelectric tracking system is a cooperative control system including multiple actuators, the traditional control method is a control strategy designed for a single actuator, forming multiple closed-loop control systems. Due to the many coupling of each actuator, the working environment and physical model are different, and with the development of technology, the number of hardware on the device is also increasing, resulting in more coupling between the various systems, greater interference and low coordination and cooperation ability, and the improvement of tracking performance has limitations [13].

Combining the advantages of distributed cooperative control, the problem of LOS stability and target tracking to be solved by the photoelectric tracking system is equivalent to the problem of consistency and robustness of cooperative control. According to the actual situation of photoelectric tracking equipment tracking the moving target, by analyzing the state of the target point movement (including position, speed and acceleration information), all executing agencies can coordinate and cooperate with each other through commands to maintain the consistency of position and speed (position deviation and speed deviation are zero), that is, the system can achieve accurate tracking [14].

The consistency conditions of the system are as follows 3.3:

$$\begin{cases} \lim_{t \to +\infty} ||x_j - x_i|| = 0 \\ \lim_{t \to +\infty} ||v_j - v_i|| = 0 \end{cases} \tag{3.3}$$

where x_i, x_j and v_i, x_j represent the position and speed of different nodes.

If the following consistency control law is selected, the following formula 3.4:

$$u_i = \sum_{j \in N} a_{ij}[(x_j - x_i) + \eta(v_j - v_i)] \tag{3.4}$$

where η represents the controller parameter, the system state equation is as follows 3.5:

$$\begin{bmatrix} \dot{X} \\ \dot{V} \end{bmatrix} = \begin{bmatrix} 0_{n \times n} & I_n \\ -L & -\eta L \end{bmatrix} \begin{bmatrix} X \\ V \end{bmatrix} \tag{3.5}$$

where $X = [x_1, \cdots, x_n]^T \in R^N, V = [v_1, \cdots, v_n]^T \in R^N$ and L are the Laplace matrices of the topological structure diagram.

3.2.2. Modeling of network structure based on leader-following . When studying the group formation control method, the pilot-following idea is simple and practical, it is also an effective method to study the consistency of collaborative control. Generally, when a group conducts group behavior movement (gathering and formation), it takes an individual in the system or an individual with leadership behavior as a leader, and other individuals as followers, through the cooperative control strategy, the position deviation and speed deviation between individuals will eventually tend to zero, which is to achieve the goal of group consistency. Unlike formation control, the performance index of consistency is that the state error between nodes is close to zero, while the constraint condition of formation control requires that the position error be constant to meet the required formation requirements.

In the photoelectric tracking system, the moving target is regarded as the leader, and each executive servo mechanism is regarded as the follower, the corresponding topological network structure is established, and the cooperative control strategy based on leader-following is researched and designed to realize the stable tracking of the photoelectric tracking system [15].

According to the matrix theory, the topological structure of the system is transformed into a matrix, and the network structure of the photoelectric tracking system is expressed in the form of matrix, such as adjacency matrix, penetration matrix, Laplace matrix, leader B matrix, etc.

Adjacency matrix: $A = \begin{bmatrix} 0 & 0 & 0 & 0 \\ 0 & 0 & 0 & 0 \\ 1 & 0 & 0 & 0 \\ 0 & 1 & 0 & 0 \end{bmatrix}$

Penetration matrix: $D = \begin{bmatrix} 0 & 0 & 0 & 0 & 0 \\ 0 & 0 & 0 & 0 & 0 \\ 0 & 0 & 0 & 0 & 0 \\ 0 & 0 & 0 & 1 & 0 \\ 0 & 0 & 0 & 0 & 1 \end{bmatrix}$

Laplace matrix: $L = D - A = \begin{bmatrix} 0 & 0 & 0 & 0 \\ 0 & 0 & 0 & 0 \\ -1 & 0 & 1 & 0 \\ 0 & -1 & 0 & 1 \end{bmatrix}$

Leader B matrix (diagonal matrix): $B = \begin{bmatrix} 1 & 0 & 0 & 0 \\ 0 & 1 & 0 & 0 \\ 0 & 0 & 1 & 0 \\ 0 & 0 & 0 & 1 \end{bmatrix}$

The tracker kinematics model is as follows:

$$\begin{cases} \dot{x}_i = v_i \\ \dot{v}_i = u_i + d_i \end{cases}, i = 1, 2, \cdots, n \tag{3.6}$$

Where, x_i and v_i represent the position and speed of the ith follower respectively, and d_i represents the disturbance to the ith follower.

The navigator kinematics model is as follows:

$$\begin{cases} \dot{x}_l = v_l \\ \dot{v}_l = u_l \end{cases} \tag{3.7}$$

The consistency performance index of the second-order collaborative control system is as follows:

$$\begin{cases} \lim_{t \to +\infty} ||x_i - x_L|| = 0 \\ \lim_{t \to +\infty} ||v_i - v_L|| = 0 \end{cases} \tag{3.8}$$

where, x_i, x_j and v_i, v_j represent the position and speed of different nodes.

If the following traditional consistency control law is selected, the following formula 3.9:

$$u_i = \sum a_{ij}[(x_j - x_i) + \eta(v_j - v_i)] + b_{ii}[(x_L - x_i) + \eta(v_L - v_i)] \tag{3.9}$$

where η represents the adjustment parameter and the element in the leader B matrix, then the closed-loop dynamic equation of the system is:

$$\begin{bmatrix} \dot{X} \\ \dot{V} \end{bmatrix} = \begin{bmatrix} 0_{n\times n} & I_n \\ -(L+B) & -\eta(L+B) \end{bmatrix} \begin{bmatrix} X \\ V \end{bmatrix} + \begin{bmatrix} 0_{n\times n} & 0_{n\times n} \\ B & \eta B \end{bmatrix} \begin{bmatrix} X_L \\ V_L \end{bmatrix} \tag{3.10}$$

where $X = [x_1, \cdots, x_n]^T \in R^N, V = [v_1, \cdots, v_n]^T \in R^N$ and L are Laplace matrices and B is leaderB matrices.

3.2.3. Consistency tracking control of finite time convergence. In the distributed cooperative control system of photoelectric tracking, fast, stable and accurate are the requirements for the stable operation of the photoelectric tracking cooperative control system. Therefore, convergence speed and accuracy can be used as performance indicators of tracking control method. Since most control algorithms are asymptotically convergent, the convergence time is particularly important for practical control systems, especially for systems requiring high control accuracy.

In order to improve the stability speed of the system, for the control strategy designed in the cooperative control system, all node states need to reach the same or the given accuracy in a limited time. Therefore, it is of great significance to study the finite-time cooperative control of photoelectric tracking system [16].

For nonlinear systems, the following formula 3.11:

$$\widehat{x} = f(x,t), f(0,t) = 0, x \in R^n \tag{3.11}$$

Considering the above nonlinear system, it is assumed that there is a C^1 smooth function $V(x)$ defined on the neighborhood $\widehat{U} \subset U_0 \subset R^n$ of the origin, and there are real numbers c>0 and 0<a<1, so that $V(x)$ is positive definite on $\widehat{U}$, $\dot{V}(x) + cV^{\alpha}(x) < 0$, then the origin of the system is stable in finite time, and its upper bound is the following formula 3.12:

$$T(x_0) \leqslant \frac{V^{1-\alpha}(x_0)}{c(1-\alpha)} \tag{3.12}$$

The real finite-time consistency convergence of the collaborative control system needs to meet the conditions, as shown in the following formula 3.13:

$$\begin{cases} \lim_{t\to T_0} ||x_i - x_L|| = 0 \\ \lim_{t\to T_0} ||v_i - v_L|| = 0 \end{cases} \tag{3.13}$$

where x_i, x_j and v_i, v_j represent the position and speed of different nodes, and T_0 is the convergence time.

The pilot-following second-order multi-agent system gives a consistent tracking control protocol based on one leader and n followers, as shown in the following formula 3.14:

$$\begin{aligned} u_i = &- [\sum a_{ij} aig^{\alpha_1}(x_i - x_j) + b_i sig^{\alpha_1}(x_i - x_l)] \\ &- [\sum a_{ij} sig^{\alpha_2}(v_i - v_j) + b_i sig^{\alpha_2}(v_i - v_l)] \end{aligned} \tag{3.14}$$

where $0 < \alpha_1 < 1, \alpha_2 = \frac{2\alpha_1}{\alpha_1+1}$.

The finite-time consistency tracking control protocol based on leadership acceleration is as follows:

$$\begin{aligned} u_i = &u_l - k_1 sig^{\alpha_1}(\sum a_{ij}(x_i - x_j) + b_i(x_i - x_l)) \\ &- k_2 sig^{\alpha_2}(\sum a_{ij}(v_i - v_j) + b_i(v_i - v_l)) \end{aligned} \tag{3.15}$$

where $0 < \alpha_1 < 1, \alpha_2 = \frac{2\alpha_1}{\alpha_1+1}. k_1 > 0, k_2 > 0.$

3.3. Finite Time Hyperspiral State Observer. The essence of the state observer is to estimate / observe variables that cannot be directly measured through the fusion of different types of information. As a virtual sensor, it provides state information feedback in real time and ensures the performance of the closed-loop control algorithm. In the actual system, because the speed information is not measurable, the system speed information can be effectively observed by designing a state observer. Considering the system (Formula 3.6) and (Formula 3.7), the following observer is defined as follows:

$$\begin{cases} \dot{\widehat{x}}_i = \widehat{v}_i + \lambda_1 sig^{\frac{1}{2}}(\widetilde{x}_i) + \lambda_2 \widetilde{x}_i \\ \dot{\widehat{v}}_i = u_i + \lambda_3 \widetilde{x}_i + \lambda_4 sgn(\widetilde{x}_i) + \widehat{d}_i \end{cases}, i = 1, 2, \cdots, n, l \tag{3.16}$$

where $\widehat{x}_i$ and $\widehat{v}_i$ are state observations and $\widehat{d}_i$ are interference estimates. Observation error $\widetilde{x}_i = x_i - \widehat{x}_i$, $\widetilde{v}_i = v_i - \widehat{v}_i$, $\widetilde{d}_i = d_i - \widehat{d}_i$. The following formula 3.17:

$$\begin{cases} \dot{\widetilde{x}}_i = \widetilde{v}_i - \lambda_1 sig^{\frac{1}{2}}(\widetilde{x}_i) - \lambda_2 \widetilde{x}_i \\ \dot{\widetilde{v}}_i = \widetilde{d}_i - \lambda_3 \widetilde{x}_i - \lambda_4 sgn(\widetilde{x}_i) \end{cases}, i = 1, 2, \cdots, n \tag{3.17}$$

Assume that the interference observation error is differentiable and bounded, that is, the following formula 3.18:

$$|\widetilde{d}_i| \leqslant \delta and |\dot{\widehat{d}}_i \leqslant \overline{\delta} \tag{3.18}$$

where $\delta > 0$, $\overline{\delta > 0}$and $\lambda_4 > \delta$. Formula 3.18 is the following formula 3.19:

$$\begin{cases} \dot{\widetilde{x}}_i = \widetilde{v}_i - \lambda_1 sig^{\frac{1}{2}}(\widetilde{x}_i) - \lambda_2 \widetilde{x}_i \\ \dot{\widetilde{v}}_i = -\lambda_3 \widetilde{x}_i - \lambda_5 sgn(\widetilde{x}_i) \end{cases}, i = 1, 2, \cdots, n \tag{3.19}$$

Among them $\lambda_5 = \lambda_4 - \delta$.

If there is real number $x_1, x_2, \cdots, x_n$ and 0<a<1, then there is: $(\sum_{i=1}^{n} |x_i|)^{\alpha} \leqslant \sum_{i=1}^{n} |x_i|^{\alpha}$.

Consider the system (equation 3.6), (equation 3.7) and observer (equation 3.16). If the assumption is true, the parameters meet the following equation 3.20:

$$\begin{aligned} \lambda_1 > 0, \lambda_2 > 2, \lambda_3 > max(o, \beta_1), \lambda_5 > max(\beta_2, \beta_3) \\ \beta_1 = \frac{9\alpha_1^2}{16\alpha_2(\alpha_2 - 2)} + \frac{\alpha_1^2 - 2\alpha_1^2\alpha_2}{2(\alpha_2 - 2)} \\ \beta_2 = \frac{9\alpha_1^2\alpha_2^2}{4\alpha_3} + 2\alpha_2^2 + 1.5\alpha_2 \\ \beta_3 = \frac{\frac{9}{16}\alpha_1^2(\alpha_2 + 0.5)^2/\alpha_2^2}{(\alpha_2(\alpha_3 + 2\alpha_1^2) - (2\alpha_3 + 0.5\alpha_1^2) - \frac{9\alpha_1^2}{16\alpha_2})(\alpha_2 - 2)} + \frac{2\alpha_2(\alpha_2 + 1)}{4(\alpha_2 - 2)} \end{aligned} \tag{3.20}$$

The system (Equation 3.17) converges to the origin in a finite time.

Proof: Order $X = [X_1, \cdots, X_n], sig^{\frac{1}{2}}(\widetilde{x}) = [sig^{\frac{1}{2}}(\widetilde{x}_1), \cdots, sig^{\frac{1}{2}}(\widetilde{x}_n)], \widetilde{v} = [\widetilde{v}_1, \cdots, \widetilde{v}_n]^T$. Consider the following Lyapunov function, as follows 3.21:

$$\begin{aligned} V_T =& \frac{1}{2} X^T X + \frac{1}{2} \widetilde{v}^T \widetilde{v} + 2\eta_3 (sig^{\frac{1}{2}}(\widetilde{x}))^T sig^{\frac{1}{2}}(\widetilde{x}) + \eta_5 x^T x \\ =& \frac{1}{2} \sum x_i^2 + \frac{1}{2} \sum \widetilde{v}_i^2 + 2\eta_3 \sum |\widetilde{x}_i| + \eta_5 \sum \widetilde{x}_i^2 \\ =& \frac{1}{2} \sum v_{ti}^2 \end{aligned} \tag{3.21}$$

where, $V_{Ti}=\frac{1}{2}X_i^2+\frac{1}{2}\widetilde{v}_i^2+2\eta_3|\widetilde{x}_i|+\eta_5\widetilde{x}_i^2=\xi_i^TP\xi_i, x_i=-\eta_1 sig^{\frac{1}{2}}(\widetilde{x}_i)-\eta_2\widehat{x}_1+\widetilde{v}_i, \xi_i=[sig^{\frac{1}{2}}(\widetilde{x}_i)\widetilde{x}_i\widetilde{v}_i]^r$, positive definite matrix is as follows 3.22:

$$P=\begin{bmatrix} 2\eta_3+\frac{\eta_1^2}{2} & \frac{\eta_1\eta_2}{2} & -\frac{\eta_1}{2} \\ \frac{\eta_1\eta_2}{2} & \frac{\eta_2^2}{2}+\eta_5 & -\frac{\eta_2}{2} \\ -\frac{\eta_1}{2} & -\frac{\eta_2}{2} & 1 \end{bmatrix} \tag{3.22}$$

The derivative of V_T is given by the following formula 3.23:

$$\begin{aligned} \dot{V}_T &= \sum \dot{V}_{Ti} = \sum \dot{\xi}_i^T P\xi_i \\ &= \sum((2\eta_3+\frac{\eta_1^2}{2})sgn(\widetilde{x}_i)\dot{\widetilde{x}}_i+2(\eta_1^2+\eta_4 s_{ti})\dot{\widetilde{x}}_i \\ &+2\dot{v}_i\dot{v}_i+1.5\eta_1\eta_2|\widetilde{x}_i|^{-\frac{1}{2}}\dot{\widetilde{x}}_i-\eta_2(\dot{\widetilde{x}}_i v_i+\widetilde{x}_i\dot{v}_i) \\ &+\eta_1(|\widetilde{x}_i|^{\frac{1}{2}}sgn(\widetilde{x}_i)\widetilde{x}_i v_i\dot{v}_i-|\widetilde{x}_i|^{-\frac{1}{2}}\dot{\widetilde{x}}_i v_i)) \\ &\leqslant \sum(-|\widetilde{x}_i|^{-\frac{1}{2}}\xi_i^TQ\xi_i+\xi_i^TM\xi_i)^{-1} \end{aligned} \tag{3.23}$$

Wherein, formula 3.24 is as follows:

$$\begin{aligned} Q=\begin{bmatrix} Q_{11} & Q_{12} & Q_{13} \\ Q_{21} & Q_{22} & Q_{23} \\ Q_{31} & Q_{32} & Q_{33} \end{bmatrix}, M=\begin{bmatrix} M_{11} & M_{12} & M_{13} \\ M_{21} & M_{22} & M_{23} \\ M_{31} & M_{32} & M_{33} \end{bmatrix} \\ Q_{11}=0.5\eta_1^3+\eta_1\eta_3, Q_{12}=Q_{21}=0, Q_{13}=Q_{31}=-0.5\eta_1^2, \\ Q_{22}=2.5\eta_2^2\eta_1-1.5\eta_1\eta_2+Q_{23}=Q_{32}=-1.5\eta_1\eta_2, Q_{33}=0.5\eta_1; \\ M_{11}=-0.5\eta_1+2\eta_1^2\alpha_2+\eta_2\eta_3-2\eta_3, \\ M_{12}=M_2M_{13}=M_{31}=-0.75\eta_1, M_{22}=\eta_2^3-\eta_2^2+\eta_2\alpha_4-2\eta_4, M_{33}=\eta_2 \end{aligned} \tag{3.24}$$

Since the matrices Q and M are positive definite, the following formula 3.25:

$$\dot{V}_{Ti}\leqslant -|\widetilde{x}_i|^{-\frac{1}{2}}\xi_i^TQ\xi_i\leqslant -|\widetilde{x}_i|^{-\frac{1}{2}}\lambda_{min}(Q)||\xi_i||^2\leqslant -\lambda_{min}(Q)||\xi_i||<0 \tag{3.25}$$

It can be seen that the following formula 3.26:

$$\dot{V}_T\leqslant \sum \dot{V}_{Ti}\leqslant -\gamma_t\sum V_{Ti}^{\frac{1}{2}} \tag{3.26}$$

where $\gamma_t\frac{\lambda_{min}(Q)}{\lambda_{max}(P)}$. Combining with lemma, the system (equation 3.2) converges to the origin in finite time, and the convergence time is as follows 3.27:

$$t_1=\frac{2V_T^{\frac{1}{2}}(\widetilde{x}(0),\widetilde{v}(0))}{\gamma_t} \tag{3.27}$$

3.4. Finite-time integral sliding mode disturbance observer. In the actual second-order cooperative control system, the dynamic performance and stability accuracy of the system are affected by the uncertain interference such as communication interference, input error and external environment. A sliding mode disturbance observer is designed to compensate the influence of disturbance on the system control effect.

The integral sliding surface is defined as follows 3.28:

$$S_{ti}=\dot{\widetilde{v}}_i+\widetilde{v}_i+\int(m_1\dot{\widetilde{v}}_i+m_2\widetilde{v}_i)d\tau \tag{3.28}$$

The interference observer is designed as follows 3.29:

$$\dot{\widehat{d}}_i=(m_1+1)\dot{\widetilde{v}}_i+m_2\widetilde{v}_i+m_3sgn(s_{ti})+m_4s_{ti}^{\omega_1}+m_5s_{ti}^{\omega_2} \tag{3.29}$$

where $m_1, m_2, m_3, m_4$and m_5 are positive real numbers. Considering the system (Equation 3.6), (Equation 3.7) and the state observer (Equation 3.16), assuming that 4.1 is true and the disturbance observer is selected (Equation 3.25), the sliding mode surface (Equation 3.24) is guaranteed to converge to zero in a finite time [17].

Proof: Order $S_T = [s_{t1}, \cdots, s_{tn}]^T, V_T = [v_{t1}, \cdots, v_{tn}]^T$. Let Lyapunov function be the following formula 3.30:

$$V_T = \frac{1}{2} S_T^T S_T = \frac{1}{2} \sum s_{ti}^2 = \sum v_{ti} \tag{3.30}$$

Take the derivative of and get the following formula 3.31:

$$\begin{aligned} \dot{V}_T = S_T^T \dot{S_T} = \sum s_{ti} \dot{s_{ti}} \\ = \sum s_{ti} (\ddot{\widetilde{v}}_i + (m_1 + 1) \dot{\widetilde{v}}_i + m_2 \widetilde{v}_i) \\ = \sum s_{ti} (\dot{d}_i - \dot{\widehat{d}}_i + (m_1 + 1) \dot{\widetilde{v}}_i + m_2 \widetilde{v}_i) \end{aligned} \tag{3.31}$$

Substitute formula 3.25 into the above formula to obtain the following formula 3.32:

$$\begin{aligned} \dot{V}_T = \sum s_i (\dot{d}_i - m_3 sgn(s_{ti}) + m_4 s_{ti}^{\omega_1} + m_5 s_{ti}^{\omega_2}) \\ \leqslant \sum (\dot{\delta} s_{ti} - m_3 |s_{ti}| - m_4 s_{ti}^{\omega_1 + 1} - m_5 s_{ti}^{\omega_2 + 1}) \\ \leqslant \sum (-(m_3 - \dot{\delta}) |s_{ti}| - m_4 |s_{ti}|^{\omega_1 + 1} - m_5 |s_{ti}|^{\omega_2 + 1}) \end{aligned} \tag{3.32}$$

When $m_3 - \dot{\delta}$, so $\dot{V} < 0$. Let $m_3 - \dot{\delta} = \phi$, formula 3.27 be the following formula 3.33:

$$\dot{V}_T \leqslant \sum (-m_3 |s_{it}|^2 - \phi |s_{ti}|) \leqslant -\phi \sum s_{ii} = -\sqrt{2} \phi (v_{ti})^{1/2} \tag{3.33}$$

Further, $\dot{V}_T \leqslant -\sqrt{2} \phi V_T^{1/2 \leqslant 0}$; Combined with Lemma 3.2, the sliding surface S_T quickly converges to zero, and the convergence time is as follows 3.34:

$$t_2 \leqslant \frac{\sqrt{2} V_T^{\frac{1}{2}} (S_{T0})}{\phi} \tag{3.34}$$

The author gives a finite-time integral sliding mode disturbance observer, which can effectively weaken the chattering and enhance the robustness of the system, so as to realize fast and accurate compensation for the overall structural disturbance of the system.

4. Result analysis. In order to verify the effectiveness of the design algorithm, the finite-time super-helix state observer, disturbance observer (Equation 3.24) and (Equation 3.23) proposed by the author are simulated and compared with ESO. The following formula 4.1:

$$\begin{cases} \dot{\widehat{x}}_i = \widehat{v}_i + \lambda_5 sig^{\omega_3} (\widetilde{x}_i) \\ \dot{\widehat{v}}_i = u_i + \lambda_6 sgn^{\omega_4} (\widetilde{x}_i) + \widehat{d}_i \\ \dot{\widehat{d}}_i = \lambda_7 sig^{\omega_5} (\widetilde{x}_i) \end{cases} , i = 1, 2, \cdots, n \tag{4.1}$$

The equivalent disturbance signal is $D = [0.5sin(2t), cos(5t), -0.6sin(20t), -0.5cos(10t)]^T$, the controller is selected (Formula 3.14), and the node level disturbance signal is $D = 0.5sin(6t)$.

Parameter design of (equation 3.16): $\lambda_1 = 3, \lambda_2 = 3, \lambda_3 = 5, \lambda_4 = 17 m_1 = 3$.

Parameter design of (equation 3.25): $m_2 = 1, m_3 = 5, m_4 = 10, m_5 = 5, \omega_1 = 0.5, \omega_2 = 1.5$.

Parameter design of (Equation 3.22) and (Equation 3.23): $c_1 = 5, c_2 = 2, \alpha_1 = 0.5, \alpha_2 = 2.5, \eta_1 = 8, \eta_2 = 3$.

The estimated error curves of the algorithm (Equation 3.16) and the interference observer (Equation 24) proposed by the author are shown in Figures 4.1 and 4.3. The ESO estimation error curve of the comparison method is shown in Figure 4.2 and Figure 4.4.

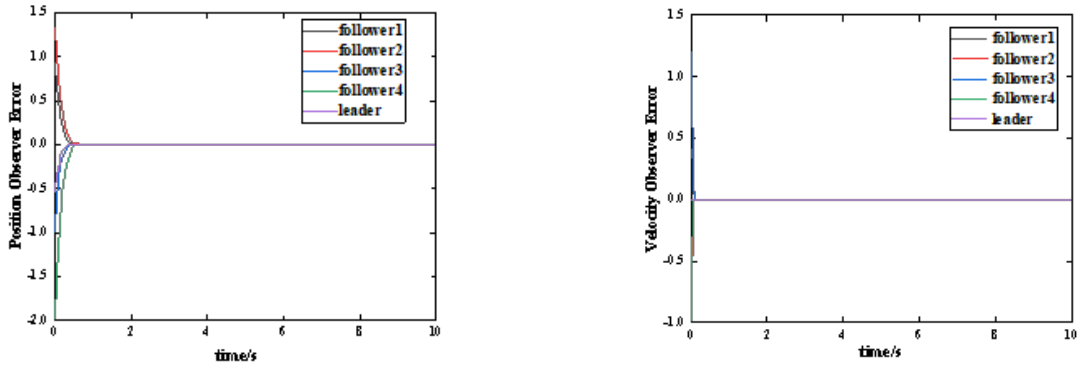

(a) Position estimation error diagram (b) Speed estimation error diagram

Fig. 4.1: State estimation error curve (Equation 3.16)

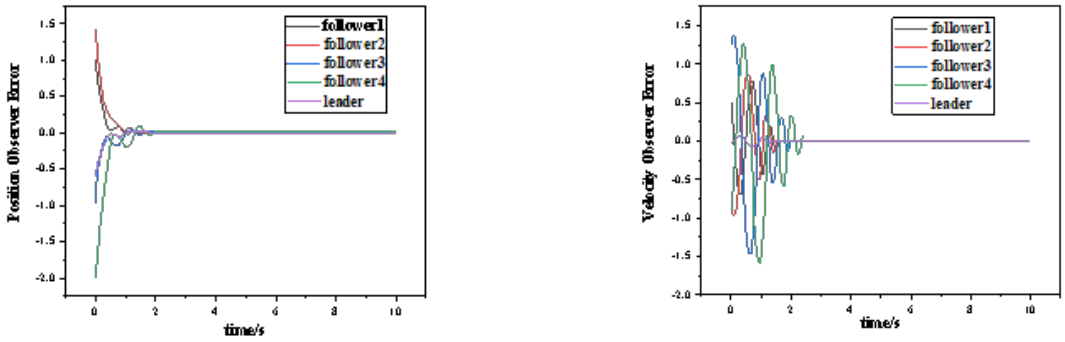

(a) ESO position estimation error (b) ESO speed estimation error

Fig. 4.2: ESO state estimation error curve

It can be seen from Figure 4.1 that the error accuracy of the system state estimation value reaches 1×10^{-8},5×10^{-6}. Estimation error range of interference observer (Equation 3.24) 5×10^{-4}. As can be seen from Figure 4.3, the position, velocity and interference estimation error accuracy of ESO respectively reach $2 \times 10^{-7}, 210^{-4}, 110^{-2}$. Through comparison, it can be concluded that the estimation error of the algorithm (formula 3.16) and the disturbance observer (formula 3.24) designed by the author are significantly smaller than the estimation error of ESO, and the buffeting is small, and they have strong compensation ability for the disturbance of different frequencies[18]. The interference estimation error range of ESO (equation 3.20) is 0.03; The interference estimation error range of (formula 3.23) designed by the author reaches 3×10^{-3}. Through comparison, it can be seen that the estimation error of (formula 3.23) designed by the author is significantly smaller than that of ESO, and the buffeting is small[19,20]. The author aims at the problem that the distributed cooperative control system does not measure the speed and has interference. First, combined with the advantages of the super-spiral anti-buffeting, a finite-time super-twisting observer (F-SO) is proposed to estimate the state information of the system structure layer quickly and accurately; Secondly, the Finite-time

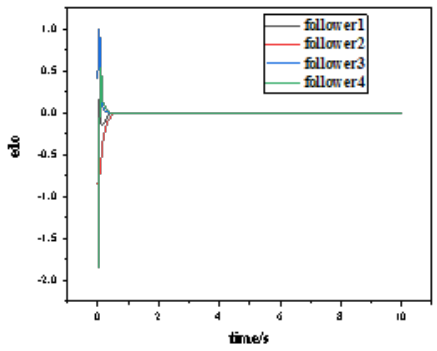

Fig. 4.3: Interference estimation error (Equation 3.16)

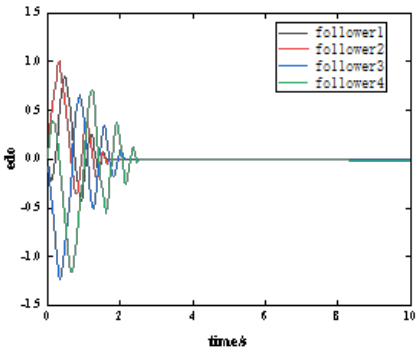

Fig. 4.4: ESO interference estimation error

Integral Siting Mode Disturbance Observer (F-ISMDOB) is designed to quickly estimate and compensate the equivalent interference, thus effectively improving the anti-interference performance of the system structure layer.

5. Conclusion. With the development of modern power electronics technology, the mobility of tracking target is enhanced, and the requirements for response speed and tracking accuracy of photoelectric tracking system are also increasing. In the industrial field, many occasions need to control the speed of electric motors. It is difficult to obtain a complex control system with multivariable and strong combination, and it is difficult to obtain good control performance. So a good control scheme is the focus of the discussion.

Aiming at the problem of obtaining unknown velocity information, the author designed a finite-time super-helix observer, which effectively estimated the system state information, and proved its stability using Lyapunov function; Aiming at the influence of system interference on system stability, the author proposes an interference observer based on integral sliding mode, estimates the interference quickly and accurately, and proves its stability.

The interference estimation error range of ESO (equation 20) is 0.03; The interference estimation error range of (formula 23) designed by the author reaches 3 × 10-3. Through comparison, it can be seen that the estimation error of (formula 23) designed by the author is significantly smaller than that of ESO, and the buffeting is small.

The author has carried out simulation analysis and compared with ESO, which fully proves the effectiveness of the observer and disturbance observer proposed by the author.

In the future, based on optoelectronics, we uses optics, precision machinery, electronics and computer technology to solve various engineering application topics. Its information carrier is being expanded from electromagnetic wave segment to optical wave segment, so that the application of photoelectric science and opto-mechanical integration technology is extended to the research direction of electrical information industry of optical information acquisition, transmission, processing, green storage, display and sensor.

Authors' contributions. The authors have made important personal contributions to this manuscript. Jing Li: writing and performing surgeries; Yunpeng Shang: data analysis and performing surgeries; article review and intellectual concept of the article.

REFERENCES

[1] Luo, Y., Xue, W., He, W., Nie, K., Mao, Y., & Guerrero, J. M. (2022). Delay-Compound-Compensation Control for Photoelectric Tracking System Based on Improved Smith Predictor Scheme. IEEE Photonics Journal, 14(3), 1-8.
[2] Bharathi, M. L., Bhatt, V., Kumar, V. R., Sharma, R. J., Hemavathi, S., Pant, B., ... & Mohanavel, V. (2022). Developing a dual axis photoelectric tracking module using a multi quadrant photoelectric device. Energy Reports, 8(8), 1426-1439.
[3] Li, J., Yuan, L., Xia, H., Huang, Y., Ma, R., Shi, J., ... & Peng, C. (2022). Rotation matrix error-decoupling methods for Risley prism closed-loop tracking. Precision Engineering, 76(1), 66-74.
[4] Maxammadovich, I. J. (2022). Design Features of Photoelectric Asymmetric Concentrators. Central Asian Journal of Theoretical and Applied Science, 3(5), 384-388.
[5] WANG, Y., & PENG, J. (2022). A Pointing Control Method of the Space Tracking Turntable Based on Extended State Observer. Spacecraft Recovery & Remote Sensing, 43(5), 78-89.
[6] Tong, W., Zhao, T., Duan, Q., Zhang, H., & Mao, Y. (2022). Non-singleton interval type-2 fuzzy PID control for high precision electro-optical tracking system. ISA transactions, 120(9), 258-270.
[7] Bao, G., Ma, L., & Yi, X. (2022). Recent advances on cooperative control of heterogeneous multi-agent systems subject to constraints: A survey. Systems Science & Control Engineering, 10(1), 539-551.
[8] Ziquan, Y., Zhang, Y., Jiang, B., Jun, F. U., & Ying, J. I. N. (2022). A review on fault-tolerant cooperative control of multiple unmanned aerial vehicles. Chinese Journal of Aeronautics, 35(1), 1-18.
[9] Shao, X., Zhang, J., & Zhang, W. (2022). Distributed cooperative surrounding control for mobile robots with uncertainties and aperiodic sampling. IEEE Transactions on Intelligent Transportation Systems, 23(10), 18951-18961.
[10] Yang, R., Liu, L., & Feng, G. (2022). An overview of recent advances in distributed coordination of multi-agent systems. Unmanned Systems, 10(03), 307-325.
[11] Liu, G., Liang, H., Pan, Y., & Ahn, C. K. (2022). Antagonistic interaction-based bipartite consensus control for heterogeneous networked systems. IEEE Transactions on Systems, Man, and Cybernetics: Systems, 53(1), 71-81.
[12] Wang, C., Ji, X., Zhang, Z., Zhao, B., Quan, L., & Plummer, A. R. (2022). Tracking differentiator based back-stepping control for valve-controlled hydraulic actuator system. ISA transactions, 119(9), 208-220.
[13] Chen, Z., Zong, X., Tang, W., & Huang, D. (2022). Design of rapid exponential integral nonlinear tracking differentiator. International Journal of Control, 95(7), 1759-1766.
[14] Wang, H., & Su, Y. (2023). Differentiator-based time delay control for uncertain robot manipulators. Asian Journal of Control, 25(1), 485-496.
[15] Gong, Y., Guo, Y., Li, D., Ma, G., & Ran, G. (2022). Predefined-time tracking control for high-order nonlinear systems with control saturation. International Journal of Robust and Nonlinear Control, 32(11), 6218-6235.
[16] Dong, H., Yang, X., Gao, H., & Yu, X. (2022). Practical terminal sliding-mode control and its applications in servo systems. IEEE Transactions on Industrial Electronics, 70(1), 752-761.
[17] Feng, H., Song, Q., Ma, S., Ma, W., Yin, C., Cao, D., & Yu, H. (2022). A new adaptive sliding mode controller based on the RBF neural network for an electro-hydraulic servo system. ISA transactions, 129(9), 472-484.
[18] Bassetto, M., Niccolai, L., Boni, L., Mengali, G., Quarta, A. A., Circi, C., ... & Cavallini, E. (2022). Sliding mode control for attitude maneuvers of Helianthus solar sail. Acta Astronautica, 198(7), 100-110.
[19] Inomoto, R. S., de Almeida Monteiro, J. R. B., & Sguarezi Filho, A. J. (2022). Boost converter control of PV system using sliding mode control with integrative sliding surface. IEEE Journal of Emerging and Selected Topics in Power Electronics, 10(5), 5522-5530.
[20] Hou, S., Wang, C., Chu, Y., & Fei, J. (2022). Neural-observer-based terminal sliding mode control: Design and application. IEEE Transactions on Fuzzy Systems, 30(11), 4800-4814.

Edited by: Bradha Madhavan
Special issue on: High-performance Computing Algorithms for Material Sciences
Received: Jan 30, 2024
Accepted: Apr 26, 2024